Okhotsk Sea and Polar Oceans Research

Volume 3 (2019)

Okhotsk Sea and Polar Oceans Research Association

Mombetsu City, Hokkaido, Japan

General Information for OSPOR

(August 2018)

1. Aims and Scope

Okhotsk Sea and Polar Oceans Research (OSPOR) is published by the Okhotsk Sea and Polar Oceans Research Association (OSPORA).

Since 1986 the Okhotsk Sea and Cold Ocean Research Association (OSCORA) has held the International Symposium at Mombetsu, Hokkaido, in Japan every February and has released its proceedings over 30 years. In 2017 OSCORA changed to OSPORA, because the Symposium scope was broadened to include the polar oceans (the Arctic and Antarctic Oceans), the Arctic passages, global warming, and environmental change in Polar Regions.

OSPORA started a reviewed papers system from the 2017 Symposium. The papers are refereed by multiple reviewers, published in the proceedings of the Symposium with a title of “Article”, and opened on the OSPOR web site.

2. Subjects covered by OSPOR

1) Environment of Okhotsk Sea
2) Meteorology and oceanography in polar regions
3) Cold region engineering
4) Arctic sea routes
5) Global warming and environment change
6) Remote sensing
7) Snow, ice and human life
8) Other topics about Okhotsk Sea and Polar Oceans

3. Editorial Policy of OSPOR

We intend to publish article papers, which should contain original scientific results and relevant subjects about Okhotsk Sea and Polar Oceans, not submitted for publication elsewhere.

4. Editorial Board

5. OSPOR website

Temporal website: http://www.o-tower.co.jp/okhsympo/top-index.html
E-mail: momsys@o-tower.co.jp

Okhotsk Sea and Polar Oceans Research
Volume 3 (2019)

Contents

Okhotsk Sea and Polar Oceans Research 3 (2019) 1-6

Article

Relationship between transpolar flights over the Arctic and the upper atmospheric circulation

Kazutoshi SATO[1] and Jun INOUE[2]

[1]Kitami Institute of Technology, Kitami, Japan
[2] National Institute of Polar Research, Tachikawa, Japan

(Received October 11, 2018; Revised manuscript accepted December 18, 2018)

Abstract

International flights from North America to Asia usually take tracks across the Arctic region for reducing fuel and operating costs. For example, the track of United Airlines flight 895 (UAL895) traveling from Chicago to Hong Kong via the Arctic region usually uses the following three routes: the Atlantic, central Arctic, and Pacific routes. Using a reanalysis product, we show that flight routes depend on the location and strength of the upper flow over the Arctic Ocean, which has a seasonal variation. During summer, when anticyclonic flow associated with blocking occurs over the Pacific Arctic region, UAL895 flights choose the Pacific and Atlantic routes to avoid a strong head wind. In addition, when the jet stream is strong over the Atlantic–Arctic region (the northern parts of Greenland and Barents Seas), the Atlantic route is selected to take advantage of strong tail winds resulting from the blocking over this region. During winter and, especially, years with less sea ice in the Bering Sea, the frequency of Alaskan blocking has increased, indicating that the prediction of the sea-ice extent over the Bering Sea would provide useful information for aircraft operation over the Arctic region.

Key words: Arctic flight track, sea-ice extent, blocking events

1. Introduction

Aircrafts contribute to the emissions of carbon dioxide (CO_2), water vapor (H_2O) and oxides of nitrogen, leading to global climate change (Lee and others 2009; 2010). Aircraft CO_2 emissions have increased to 2.5% of the total anthropogenic emitted CO_2 over the previous 50 years (Lee and others 2009). The strengthened column-averaged, north–south temperature-gradient response to the increase in CO_2 has caused an increased level of upper-level clear-air turbulence, which is a major cause of aviation incidents (e.g., injured passengers, structural damage, flight delays) (Sharman and others 2006). Previous studies have reported an increase in the frequency and intensity of turbulence at upper levels for a doubling of the CO_2 concentration (Williams and Joshi 2013, Williams and others 2017, Storer and others 2017). A reduction in fuel usage would, therefore, help to reduce operating costs and minimize climate impacts.

Two approaches to reduce aircraft emissions are the development of technologies (e.g., efficient engines, clean fuels, body and wing forms) and the improvement of air-traffic management (e.g., shortening flight times), which may be optimized by monitoring the upper atmospheric circulation, because aircraft routes and flight lengths mainly depend on the horizontal wind speed at upper levels (Palopo and others 2010). Therefore, avoiding headwinds and enhancing the probability of tailwinds would reduce aircraft fuel consumption. Previous studies have reported that the change in the phase of atmospheric circulation over the Atlantic sector causes changes in the position and strength of the jet stream, and thereby influences aircraft routes (Irvine and others 2013; Kim and others 2016; Williams 2016). Kim and others (2016) indicated certain links between the route and travel time of a flight from New York to London and the phase of the North Atlantic Oscillation (NAO). In the positive phase (NAO+), when the jet stream tends to shift northward over the northern Atlantic Ocean, flight times become shorter than during the negative phase (NAO-). In addition, the number and timing of the route varies with the season because of differences in the strength and location of the jet stream in summer and winter (Irvine and others 2013). In contrast, over the Pacific Ocean, changes in atmospheric circulation over high and low latitudes (e.g., resulting from the Arctic and El Niño Southern Oscillations) affect the flight time of aircraft at mid-latitudes (Karnauskas and others 2015). Therefore, the route and season are strongly influenced by atmospheric circulation patterns over the Northern Hemisphere.

Polar routes exist to minimize the total travel time and fuel consumption of aircraft travelling from one continent to another. The commencement of cross-polar flight began in 1998 when entry into Russian airspace was permitted by the Russian Government (Jacobson and others 2011). The number of international flights that use the Arctic route has been increasing in recent decades, with several companies currently using the cross-polar flight track throughout the year.

The United Airlines (UAL) flight 895 travels from Chicago (ORD) to Hong Kong (HKG) almost every day, which, to minimize the distance and time of flight, passes over the Arctic region (Fig. 1a). However, flight UAL895 does not always travel the shortest route from ORD to HKG, suggesting the dependence of the Arctic route on the upper level flow over the Arctic Ocean. We investigate here the relationship between the flight track and the upper-level atmospheric circulation, particularly during the summer and winter seasons.

2. Data and methodology

2.1 Meteorological data

We use 6-h ERA-Interim reanalysis data from January 1979 to December 2016 on a 0.75° × 0.75° latitude/longitude grid produced by the European Centre for Medium-Range Weather Forecasts (Dee and others 2011) for determination of the geopotential height, wind speed, sea-surface temperature, and sea-ice concentration. We mainly focus on the atmospheric circulations during summer (from May to August, hereafter MJJA) and winter (from December to March, hereafter DJFM). To calculate the frequency of blocking events over the Northern Hemisphere, we apply a blocking index defined by D'Andrea and others (1998). At each longitude, the meridional gradient of geopotential height at 250 hPa (Z250) between the southern and northern parts of Z250 (*GHGS* and *GHGN*) are calculated as

$$GHGS = Z(\psi_0) - Z(\psi_s) / (\psi_0 - \psi_s) \tag{1}$$

and

$$GHGN = Z(\psi_n) - Z(\psi_0) / (\psi_n - \psi_0) \tag{2}$$

respectively, where

$$\begin{aligned} \psi_n &= 76.5°\pm\Delta \\ \psi_0 &= 60.0°\pm\Delta \\ \psi_s &= 43.5°\pm\Delta \end{aligned} \tag{3}$$

for Δ= 0°, 0.75°, 1.5°, 2.25°, 3.0°, 3.75°, 4.5°.

A specific longitude on a given day is locally defined as being blocked if both of the following conditions are satisfied (for at least one value of Δ):

$$GHGS > 0 \tag{4}$$

and

$$GHGN < -5 \text{ m/(degrees latitude)} \tag{5}$$

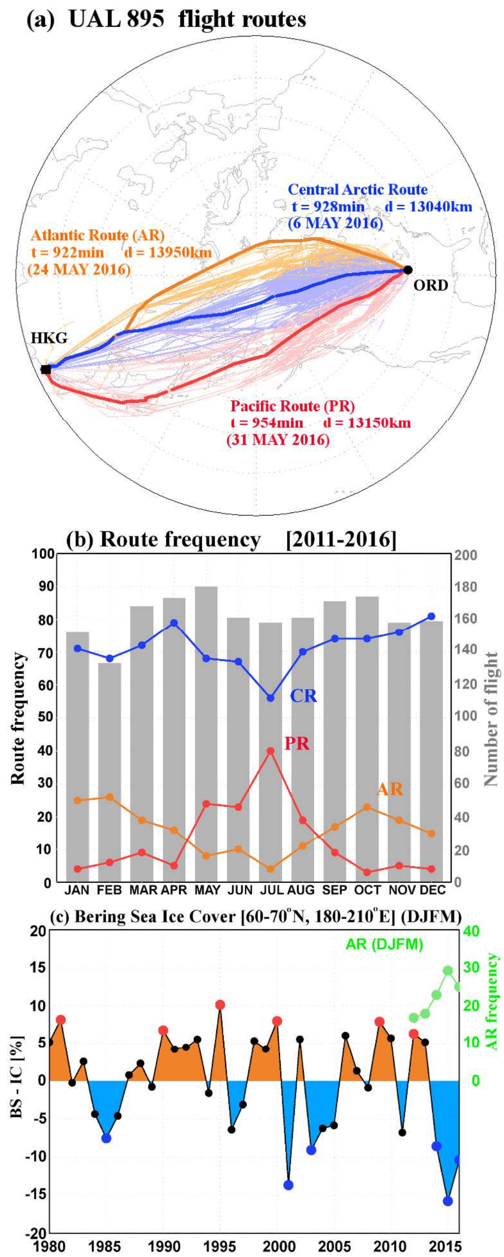

Fig. 1 (a) All flight tracks (thin lines) and the representative track (thick lines) for the Atlantic (AR, orange), central Arctic (CR, blue) and Pacific routes (PR, red) for May 2016. The time and distance for the representative tracks are shown.

(b) Monthly average frequency of each route from 2011–2016. Gray bars show the number of flights from Chicago (ORD) to Hong Kong (HKG) via the Arctic region from 2011–2016.

(c) Ice-cover anomaly during December and March from the climatology over the Bering Sea (60–70°N, 180–210°E) from ERA-Interim. The green line shows the frequency of flights taking the Atlantic route.

2.2 Flight track data

Flight information is obtained from the flightaware website (https://flightaware.com), which provides the location, height and total flight time of commercial flights all over the world. We focus on flight UAL895 from ORD to HKG over the Arctic region (Fig. 1a), whose average total flight time is about 16 h depending on the flight track. Flight information is available since 2011, which is a relatively long time period compared with other flights for this route.

We use the northernmost position of aircraft over the Atlantic (15°W–15°E) and Pacific (165°E–165°W) Arctic regions to classify UAL895 flight tracks, resulting in three routes: the Atlantic route (northward of 75°N over the Atlantic–Arctic region or northward of 87°N over the Pacific–Arctic region), the central Arctic route (from 72°N to 87°N over the Pacific–Arctic region) and the Pacific route (southward of 72°N over the Pacific–Arctic region). Examples of flight tracks for each route in May 2016 are shown in Fig. 1(a). As the central Arctic route is the most efficient and shortest route between ORD and HKG, it is the most common of the three routes throughout the year (Fig. 1(b)). Both the Atlantic and Pacific routes have a longer distance compared with the central Arctic route, however, flight UAL895 sometimes chooses them at a frequency depending on the season. While the Pacific route has a higher frequency during MJJA, the Atlantic route has a higher frequency during DJFM, indicating that the aircraft routing over the Arctic region depends on the atmospheric circulation and season.

3. Relationship between the Arctic flight route and upper-atmospheric circulation

3.1 Summer

During summer, flight UAL895 chooses the central Arctic or Pacific routes almost exclusively (Fig. 1(b)). To understand the difference in upper atmospheric circulation patterns between the central Arctic and Pacific routes, we constructed maps of geopotential height and wind speed at 250 hPa (Z250 and W250) by subtracting the composites of central-Arctic-route days from those of Pacific-route days during summer. Figure 2(a) shows the differences in Z250 and W250 between the Pacific- and central-Arctic-route days during summer, with positive anomalies of Z250 found over the Pacific–Arctic sector. The head-wind anomalies from far eastern Eurasia to the Canadian Arctic Archipelago are consistent with an anticyclone flow associated with positive Z250 anomalies. In contrast, the tail-wind anomalies associated with positive Z250 anomalies are seen from eastern Asia to Canada. Therefore, the Pacific route is very favorable for flight UAL895 when the head wind over the Pacific–Arctic region is strengthened, and the tail-wind anomaly is strong from Alaska to eastern Asia.

The positive anomalies of Z250 suggest the increase in the frequency of summer blocking over eastern Asia and the Beaufort Sea during Pacific-route days. The peak blocking events over the European–Atlantic and Pacific regions are significant weather events according to previous studies (Matsueda 2009, Matsueda and Endo 2017, Hoffman and others 2014). We show the difference in the frequency of summer blocking events between the central-Arctic-route and Pacific-route days in Fig. 3(a), where, over the Pacific region (around 150°E and 130°W), two peaks of the difference in the frequency of blocking are clearly seen. The increases in the blocking frequency are consistent with a positive Z250 anomaly over eastern Asia and Alaska/northern Canada (Fig. 2(a)). When the blocking dominates over the Pacific–Arctic region, flight UAL895 takes the Pacific route to avoid the strong head wind associated with this blocking pattern. This result suggests that the blocking events over the Pacific–Arctic regions and eastern Asia are the fundamental phenomena governing flight routes during summer.

3.2 Winter

We focus on the difference in atmospheric circulation between the central Arctic and Atlantic routes, where the latter is more frequent during winter (Fig. 1(b)). Using the same composite maps as in Fig. 2(a), but focusing on the winter case (Fig. 2(b)), we see that for Atlantic-route days, positive Z250 anomalies appear over Alaska and western Canada, causing head-wind anomalies from the central Arctic to the Canadian Arctic Archipelago. In contrast, tail-wind anomalies exist from northern Greenland to central Siberia. The positive Z250 anomaly dominates over the Barents Sea, enhancing anticyclonic flow at the upper level. For Pacific-route days, positive Z250 anomalies are found over Alaska and western Canada, however, a positive W250 anomaly is not clearly seen over the Barents Sea (not shown).

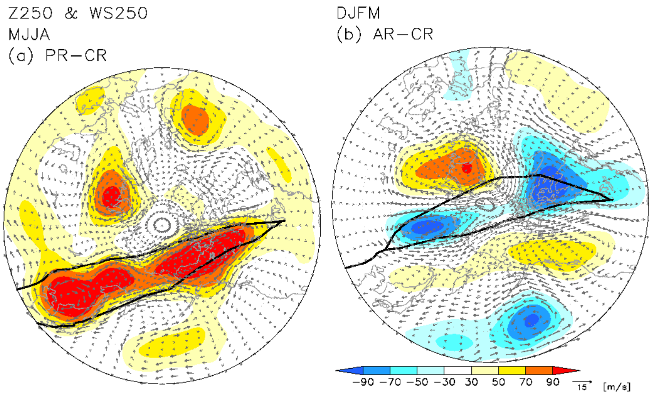

Fig. 2 (a) Difference maps in geopotential height (Z250 [m]: shading) and air velocity (vectors [m/s]) at 250 hPa between the Pacific (PR) and central Arctic (CR) routes for summer (MJJA).
(b) Difference maps in geopotential height (shading [m]) and velocity (vectors [m/s]) at 250 hPa between the Atlantic (AR) and central Arctic routes for winter (DJFM). Black contours show the representative tracks as shown in Fig. 1a.

During winter, relatively higher blocking frequencies are found over the European–Atlantic and Pacific sectors for Atlantic-route and central-Arctic days. There is a difference in blocking frequencies over the European–Atlantic sector (between 20°E and 50°E) and the Pacific region (between 150°E and 130°W) in winter (Fig. 3b), although the amplitude of difference is smaller than that in summer. The peak European–Atlantic (Pacific) blocking difference results from a positive anomaly of Z250 over the Barents Sea (from Alaska to western Canada), suggesting that the winter blocking over the Pacific and European–Atlantic sectors impacts the aircraft route over the Arctic Ocean.

3.3 Atmospheric response to change in Arctic sea ice

The decline in Arctic winter sea ice promotes turbulent heat release into the atmosphere, resulting in a geopotential height anomaly over the Arctic region (Rinke and others 2013). To understand the atmospheric response to sea-ice decline over the Arctic, we focus on years with low and high sea-ice extent in the Bering Sea (Fig. 1(c)), and investigate the difference in the atmospheric circulation in Z250 fields during winter (Fig. 4(a)). The Z250 anomaly pattern is similar that for Atlantic-route days as shown in Fig. 2(b), particularly for the Western Hemisphere, indicating that this anomaly pattern may be a response to the decline in Bering Sea ice. In fact, the frequency of Atlantic-route days during winter was relatively high during years of low ice extent (the winters of 2015 and 2016), while in years with a high ice extent (the winters of 2012 and 2013), the frequency was relatively low compared with other years. To investigate the relationship between the sea-ice extent over the Bering Sea and the atmospheric circulation over the Northern Hemisphere, we performed regression analyses between Z250 and the sea-ice concentration over the Bering Sea (Fig. 4(b)), giving a positive correlation over western Canada and a negative correlation over the North Pacific. This pattern of Z250 is similar to patterns of the Z250 anomaly during years with a low ice extent (Fig. 4(a)) and Atlantic-route days (Fig. 2(b)), although the amplitude of Z250 is smaller than for Z250 anomalies in Figs. 2(b) and 4(a), indicating that the increased Alaskan blocking frequency during years with a low ice extent influences flight operations.

For composite maps as in Fig. 4(a), but focusing on the summer case, the Z250 anomaly pattern is different from the winter case in terms of the atmospheric response to sea-ice decline over the Bering Sea (not shown), because anomalous snow melting in northern Eurasia leads to summer atmospheric circulation anomalies (Matsumura and others 2010). Matsumura and Yamazaki (2012) found that large surface heating associated with early snow melting in northern Eurasia forms an anticyclonic circulation anomaly over eastern Siberia. In addition, the El Niño-Southern Oscillation and the development of the Okhotsk High determine the degree of summer blocking over the eastern Asia region (Park and Ahn 2014).

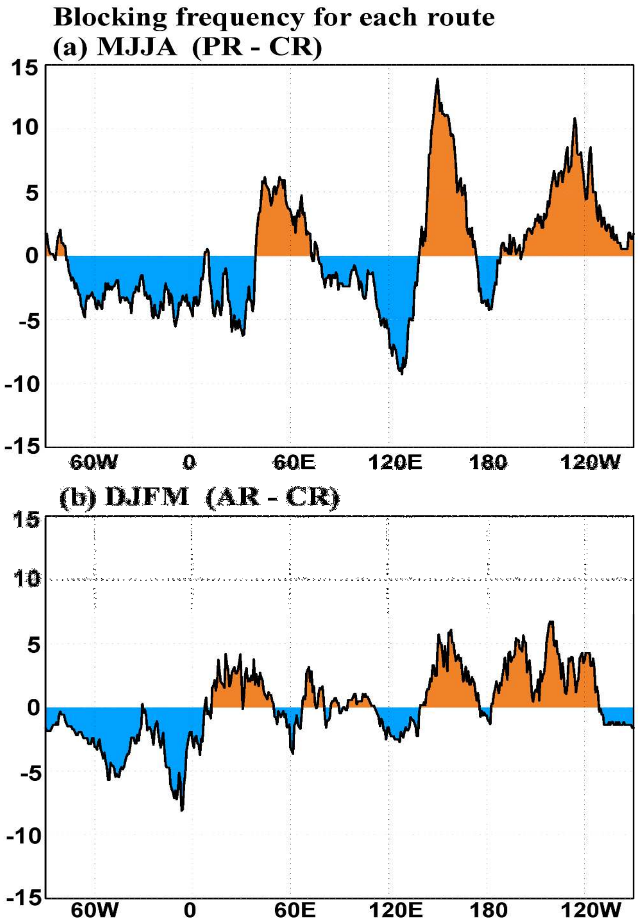

Fig. 3 (a) Difference in frequency of blocking [%] between the Pacific (PR) and central Arctic (CR) routes (PR-CR) in summer (MJJA) as a function of longitude.

(b) Difference in frequency of blocking [%] between the Atlantic (AR) and central Arctic (CR) routes (AR-CR) in winter (DJFM) as a function of longitude.

4. Summary and discussion

We have investigated the relationship between the upper level flow over the Northern Hemisphere and flight tracks over the Arctic region. The tail wind anomaly from northern Greenland to western Siberia is induced by European–Atlantic blocking, which influences flight operations during winter. Alaskan blocking events during summer, which result in a head-wind anomaly from eastern Siberia to the Canadian Arctic Archipelago, impede aircraft from crossing the central Arctic route, while the tail wind anomaly from Alaska to eastern Asia is favorable for the Pacific route. Our composite analysis demonstrates the impact of blocking events on aircraft routes.

However, operational and fuel costs must be discussed before the beneficial operation of flights can be considered. Operational costs not discussed here include the cost of entering another country's airspace, which differs for each country. Previous studies have reported that the increased probability of a tail wind minimizes the total flight time, and reduces the fuel and operational costs (Williams 2016, Karnauskas and others 2016, Kim and others 2016). Based on results of these studies, using the tail wind anomaly from northern Greenland to western Siberia and over the Pacific Ocean, while avoiding the head wind anomaly area from eastern Siberia to the Canadian Arctic Archipelago, would reduce operational and fuel costs. Hence, the accurate forecast of blocking events is important for aircraft operation over the Arctic region.

The frequency of summer Pacific blocking events from 2051 and 2110 is expected to increase slightly (Matsueda and Endo 2017). In addition, Pacific blocking events lasting 15–29 days are predicted to increase in the future, suggesting that planning would be simplified because once a blocking situation develops, the atmospheric pattern likely persists for weeks, which favors the Pacific route. In contrast, winter blocking events lasting 9 days or less are expected to increase in the future. Our results show that the frequency of the Alaskan blocking event is related to the sea-ice concentration over the Bering Sea, and would be the determining factor during years with a low sea-ice extent in the Bering Sea. An accelerated decline in the Arctic sea ice would lead to an increase in the frequency of Alaskan blocking events, which would continue to influence aircraft operation over the Arctic region in the future.

As the sea-ice retreat in the Bering Sea is predictable through the 3-month leading Z500 (Nakanowatari and others 2015), the forecasting of sea-ice variability would provide an efficient guide for aircraft operations over the Arctic Ocean. However, the amplitude of the Z250 anomaly associated with sea-ice decline is smaller than that of the difference in Z250 between years with a low and high ice extent, implying that the Z250 anomaly is not entirely explained by the decline in Arctic sea ice. For example, the change in sea-surface temperature over the mid-latitudes has a large impact on storm tracks in the Northern Hemisphere, resulting in a wind-speed anomaly over the Arctic region (Sato and others 2014, Ok and others 2017). Screen and Francis (2014) suggested that the atmospheric response to the variability of sea-surface temperature over tropical ocean causes the wind-speed and temperature anomalies at higher latitudes. Therefore, sensitivity experiments must be performed to investigate the atmospheric response to a change in the sea-surface temperature over mid-latitudes and the tropics in the near future.

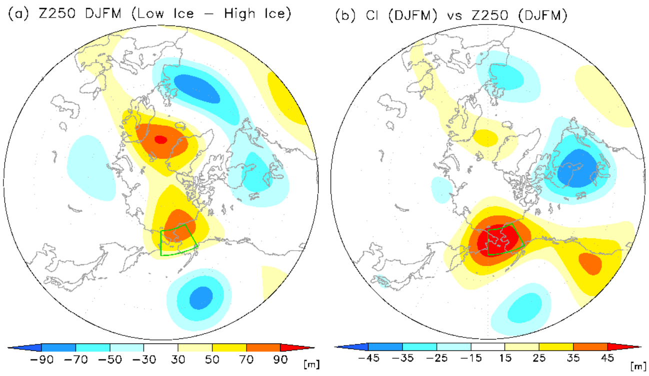

Fig. 4 (a) Difference maps in Z250 between years with low and high sea-ice extent in the Bering Sea for winter (DJFM).
(b) Regression field of Z250 with Bering Sea ice cover in winter.

Acknowledgements

This work was supported by a Grant-in-Aid for Scientific Research (KAKENHI(A) 18H03745) and the Arctic Challenge for Sustainability (ArCS) project. We would like to thank anonymous reviewers whose constructive comments improved the quality of this manuscript. We used United Airline 895 flight information from Flightaware (https://flightaware.com). We thank Richard Foreman, PhD, from Edanz Group (www.edanzediting.com/ac) for correcting a draft of this manuscript.

References

D'Andrea F., and 16 others (1998): Northern Hemisphere atmospheric blocking as simulated by 15 atmospheric general circulation models in the period 1979–1988. *Clim. Dyn.*, **14,** 385–407, doi:10.1007/s003820050230.

Dee, D.P. and 35 others (2011): The ERA-Interim reanalysis: configuration and performance of the data assimilation system, *Q. J. R. Meteorol. Soc.*, **137**, 553–597.

Hoffman, H.N. and W. Zhou (2014): Implications of Ural blocking for East Asia winter climate in CMIP5 GCMs. Part I: Biases in the historical scenario, *J. Clim.*, **28**, 2203-2216, doi: 10.1175/JCLI-D-14-00308.1.

Irvine, E. A., B.J. Hoskins, K.P. Shine, R.W. Lunnon and C. Froemming (2013): Characterizing North Atlantic weather patterns for climate-optimal aircraft routing, *Meteorol. Appl.*, **20**, 80–93.

Jacobson, M.Z., J.T. Wilkerson, S. Balasubramanian, W.W.Jr. Cooper and N, Mohleji (2012): The effects of rerouting aircraft around the arctic circle on arctic and global climate, *Climatic Change*, **115**, 709–724, doi:10.1007/s10584-012-0462-0.

Karnauskas, K.B., J.P. Donnelly, H.C. Barkley and J.E. Martin (2015): Coupling between air travel and climate, *Nat. Clim. Change*, **5**, 1068–73.

Kim, J.-H., W.N. Chan, B. Sridhar, R.D. Sharman, P.D. Williams and M. Strahan (2016): Impact of the North Atlantic Oscillation on transatlantic flight routes and clear-air turbulence, *J. Appl. Meteor. Climatol*, **55**, 763-771.

Lee, D.S., D.W. Fahey, P.M. Forster, P.J. Newton, R.C.N. Wit, L.L. Lim, B. Owen and R. Sausen (2009): Aviation and global climate change in the 21st century, *Atmos. Environ.*, **43**, 3520–3537.

Lee, D. S., G.Pitari, V. Grewe, K. Gierens, J.E. Penner, A. Petzold, M.J. Prather, U. Schumann, A. Bais, T. Berntsen, D. Iachetti, L.L. Lim and R. Sausen (2010): Transport impacts on atmosphere and climate: aviation, *Atmos. Environ.,* **44,** 4678–4734.

Matsueda, M. (2009): Blocking predictability in operational mediumrange ensemble forecasts, *SOLA,* **5**, 113–116.

Matsueda, M. and H. Endo (2017): The robustness of future changes in Northern Hemisphere blocking: A large ensemble projection with multiple sea surface temperature patterns *Geophys. Res. Lett,,* **44**, 5158–5166, doi:10.1002/2017GL073336.

Matsumura, S., K. Yamazaki and T. Tokioka (2010): Summertime landatmosphere interactions in response to anomalous springtime snow cover in northern Eurasia, *J. Geophys. Res.,* **115**, D20107, doi :10.1029/2009JD-12342.

Matsumura, S. and K. Yamazaki, (2012): Eurasian subarctic summer climate in response to anomalous snow cover, *J. Clim*, **25**, 1305–1317.

Nakanowatari, T., J. Inoue, K. Sato and T. Kikuchi (2015): Summertime atmosphere-ocean preconditionings for the Bering Sea ice retreat and the following severe winters in North America, *Environ. Res. Lett.,* **10**, 094023, doi: 10.1088/1748-9326/10/9/094023.

Ok, J., M.K. Sung, K. Sato, Y.K. Lim, S.J. Kim, E.H. Baek, J.H. Jeong and B.M. Kim (2017): How does the SST variability over the western North Atlantic Ocean control Arctic warming over the Barents/Kara seas? *Environ. Res. Lett.,* **12**, 034021.

Palopo, K., R.D. Windhorst, S. Suharwardy and H.-T. Lee (2010): Windoptimal routing in the national airspace system, *J. Aircr.,* **47**, 1584–1589.

Park, Y.J. and J.B. Ahn, (2014): Characteristics of atmospheric circulation over East Asia associated with summer blocking *J. Geophys. Res. Atmos.,* **119**, 726–738, doi:10.1002/2013JD020688.

Rinke, A., K. Dethloff, W. Dorn, D. Handorf and J.C Moore (2013): Simulated Arctic atmospheric feedbacks associated with late summer sea ice anomalies, *J. Geophys. Res.,* **118**, 7698–7714.

Sato, K., J. Inoue and M. Watanabe (2014): Influence of the Gulf Stream on the Barents Sea ice retreat and Eurasian coldness during early winter, *Environ. Res. Lett.,* **9**, 084009, doi:10.1088/1748-9326/9/8/084009.

Screen, J.A. and J.A. Francis (2016): Contribution of sea-ice loss to Arctic amplification is regulated by Pacific Ocean decadal variability, *Nat. Clim. Change*, **6**, 856-860.

Sharman, R., C. Tebaldi, G. Wiener and J. Wolff, (2006): An integrated approach to mid- and upper-level turbulence forecasting, *Weather Forecast*, **21**, 268–287.

Storer, L.N., P.D. Williams and M.M. Joshi, (2017): Global response of clear-air turbulence to climate change, *Geophys. Res. Lett.*, **44**, 9976–9984, doi:10.1002/2017GL074618.

Williams, P.D. and M.M Joshi (2013): Intensification of winter transatlantic aviation turbulence in response to climate change, *Nat. Clim. Change,* **3**, 644-648.

Williams, P. D. (2016): Transatlantic flight times and climate change, *Environ. Res. Lett.,* **11**, 024008, doi: 10.1088/1748-9326/11/2/024008.

Williams, P.D. (2017): Increased light, moderate, and severe clear-air turbulence in response to climate change. *Adv. Atmos. Sci.*, **34**(5), 576–586, doi: 10.1007/s00376-017-6268-2.

Summary in Japanese

和文要約

北極海空路と北半球の大気循環場との関係

佐藤和敏 [1], 猪上淳 [2]

[1] 北見工業大学, [2] 国立極地研究所

北アメリカ-アジア間で運行されている国際線は、エネルギー消費や飛行時間を抑えるため、距離の短くなる北極海の上空を通過する。シカゴ-香港間で運行されているユナイテッド航空 895 便（UAL895）は、北極海の上空を通過する航空機の1つだが、北極海上を通過する空路は主に 3 つ（太平洋側ルート、中央北極海ルート、大西洋側ルート）に分類することができる。これは、飛行機は上空の追い風を受けることで、飛行時間を短縮できるためである。そこで本研究では、再解析データを用いて、北半球のブロッキングに伴う風の強さや位置の変化と UAL895 が北極海上を飛行するルートに関係があることを明らかにした。北半球では、ブロッキングに伴い北極海太平洋側で高気圧性の循環が強まると、北極海中央で向かい風が強くなるため、航空機が北極海の大西洋側や太平洋を通過する傾向にある。一方、大西洋側北極海でブロッキングに伴い上空の風が強まると、グリーンランド上空で追い風が強くなるため、大西洋側北極海を通過する傾向にあった。北極海の上空の大気循環は、熱帯の海面水温やベーリング海の海氷分布と関係性が見られており、数ヶ月前から予報可能であることが示唆され、北極海ルートを通過する航空会社に有益な情報を提供できる可能性がある。

Okhotsk Sea and Polar Oceans Research 3 (2019) 7-12

Article

Utilization of discarded and unused woody materials for biomass heating and power plant

Tsuyoshi YODA[1,2]

[1] *City Mombetsu, Mombetsu, Japan*
[2] *Hirosaki Industrial Research Institute, Aomori Prefectural Industrial Technology Research Center, Hirosaki, Japan*

(Received June 5, 2018; Revised manuscript accepted December 25, 2018)

Abstract

The global warming due to increases of warming gases in the atmosphere has well been recognized in the world. Reducing the emission of CO_2 is crucial now for every nation together with its regional governments. As biomass energy resources, discarded and unused woody materials from local forests will be one of the solutions, as the trees have consumed a great amount of CO_2 through the lifetime and they will emit nearly equal amount of CO_2 when burning, and the CO_2 liberated from their burning might be able to be isolated from the atmosphere into storage. The economic aspects are always key issue in biomass energy. Putting stress on the economic aspects of biomass energy, the author studied the biomass fuels for heating units and power plants on its present state and future prospective, in a local city in Hokkaido, northern island of Japan, where cold and frequent heavy snowing are typical in winter.

Key words: biomass energy, discarded wood, unused wood, heating, power plant

1. Background

Energy shortage such as oil and gas has featured Japan, where the society and industry have long covered it by import from rich countries in natural energy. Coal, abundantly reserved in Japan, is only an exception. However, unfortunately, most of coal found in deep under-ground layers has been defeated in its market by oversea cheap ones produced from opencast mines, and even coal has been imported.

Mountainous nature with few long and magnificent rivers and narrow continental shelves, has impeded development of water, tidal and wind forces as typical renewable energy. Contrary to the U.S. and other large countries, mountainous country does not directly mean rich in usable biomass reserves, particularly in wood, since the steep mountains often bring about relatively high market prices of those woody products, in particular, of discarded wood in forests.

The global warming due to increases of warming gases in the atmosphere has well been recognized in the world. Reducing the emission of CO_2 is crucial now for every nation together with its regional governments, through overcoming any hindrance and negative background. As biomass energy resources, discarded and unused woody materials from local forests will be one of the solutions, as the trees have consumed a large amount of CO_2 through the lifetime and they will emit nearly equal amount of CO_2 when burning, and the CO_2 liberated from their burning might be able to be isolated from the atmosphere into storage. As an alternative fuel from local forests will be one of the solutions, as the forest has consumed a great amount of CO_2 through its lifetime and it will emit the equal amount of CO_2 when burning and the CO_2 liberated from its burning might be able to be isolated from the atmosphere in storage. It will have an opportunity to bring great benefits to the environment with some measures to reduce the amount of the emission greatly. The energy stored in wood is able to be converted into useful energy by transferring heat from combustion to hot water, where boilers play key role. Biomass boilers have been developed in the world as alternative heating source generators to coal boilers (Saidur and others, 2011, for an instance).

Biomass boilers are used for heating buildings; industrial premises, central and municipal heating plants, farm building, hotels, operating facilities, etc. In Hokkaido, biomass boilers have widely been in use (Kuboyama, and others, 2004; Official Website of Hokkaido Prefecture 2018a, 2018b; Niseko's Towns efforts as an Eco Model city).

Eventually, the forest should be properly managed to keep it well in order to sustainable use of biomass woody materials, and to prevent illegal deforestations and any harmful activity, certificate systems should be requested for forest enterprises and performing parties and persons, together with related regulations (Yamamoto and others, 2014). The Sustainable Green Ecosystem Council (SGEC) established in 2003 provides a unique certificate system for forest sustainability, which is oriented toward the peculiar situation in Japan, where afforestation prevails and a number of small size forest owners holds a majority in its society. SGEC has controlled the amount of logging activity per year and area, ordered forestations after logging, and set up forestation plans and their road maps to future.

In the wider definitions, biomass includes agricultural and food processing wastes as well as sewage sludge and animal manure. The paper does not take considerations about them. Two clear reasons exist. One of them is that the amount of those fuel sources could not be available in cities of relatively small size in populations. The other is that the total amount of discarded wood over Hokkaido is about 110mil.m^3, of which 40 mil. m^3 is utilized as biomass energy source at the present. There remains considerable amount of discarded woods to be able to alter to active energy.

There are a few kinds of biomass fuels that come from local forests. They are wood pellets, precision dry wood chips, green wood chips, and general discarded wood chips. The main differences between them will be moisture content, calorific value, bark percentage, the amount of processing each one goes through, and the price as a consequence. The wood pellets, most energy dense one, usually contain a moisture between 5% and 8%, and they are the driest and easiest to manage. However, the pellets need large forest resources and slightly big consumer markets. Discarded wood chips will include the byproduct pieces and chips of lumbering, which are slightly different from the discarded ones in forests.

In the local city the present paper discusses, for the moment at least, the consumer market is not large enough for the pellets to be appropriate for purposes of heating and/or power generation. In the discarded wood, the bigger ones are the more useful as fuels. When the marketable timbers are taken away from the forest, the bigger ones are usually left in the forest, due to the cost to remove them, and as a consequence, they remain as obstacles for afforestation in the forest.

The biomass fuel resources are found abundant in regional forests in Hokkaido. For instance, the Official Website of Hokkaido Prefecture(2018b) noted the amount 1,110,000 m^3/year of them was left in the Hokkaido prefecture. Such large amount of discarded wood left in the forests aroused the interest of the regional researchers, to generate energy for heat through boilers for the regional societies. They soon found the transport cost of the discarded wood from the forests to boilers caused a main hindrance in this renewable energy usage, which included secure of transport measures, including preparing devices to transport them. The transport measures are often expensive. Both national and regional governments support the project by purchasing main particular devices and/or granting subsidies to the enterprises. Up to the present, the society of Japan has relied on imported fossil fuels to large extent. Although fossil fuels have higher calorific value per kg. and easy to manage, their prices have been unstable and fossil fuel resources are of limited amount of resources.

A previous study investigated the economic aspects of biomass related ecosystems (Bateman and others, 2011). However, the society and the market discussed in it are different from those of the present study. The economic aspects are always key issue in biomass energy. On the economic point of view of energy, the author studied the biomass fuels for heating units and power plants on its present state and future prospective, in a local city in Hokkaido, northern island of Japan, where cold and frequent heavy snowing are typical in winter.

2. Government policies for biomass utilization in Japan

To promote the renewable energy production and biomass utilization for heat and power generation, Japan has established a number of policies and incentives. Basic Act for the promotion of biomass utilization in 2009, its Amendment(2016) and Basic Plan for the promotion of biomass utilization in 2010 were aimed to set basic policies on the development of technologies for biomass utilization. The most critical policy was “Feed-in Tariff Scheme for Renewable Energy (Ministry of Economy, Trade and Industry:METI) which has been implemented since July 2012, soon after the tragic Tohoku Earthquake and Fukushima nuclear power plant accident. Since then, wood pellet consumption in Japan has grown up.

According to FAOSAT in 2016, the domestic production of wood pellets in the last five years was only 90t, most of which were exported to the market of China, and relatively high quality pellets, which covered a larger consumption of pellets in Japan, have been imported from Canada, China, Vietnam and the others.

To prevent illegal logging for wood pellets on the sustainable forest principle, the Basic Act for the Promotion of Biomass Utilization has a number of requirements for wood pellets and the other biomass use. Some of them are noted as follows:

·Mitigation of global warming,

·Revitalization of rural areas,

·Full utilization of different types of biomass,

·Considerations of environment preservation.

Under the Ministry of Agriculture, Forestry and Fisheries’ (MAFF) slogan, “illegal harvested timber should not be used”, the Clean Wood Act went into force in 2017, since illegal imports of wood products through complex trade routes had not been blocked.

As to wood chips, the standardizations are still at the development stage, probably due to no notable trading market in Japan for the moment.

3. Methodology

3.1 Calorific values of wood chips

Among a variety of kinds of tree, Japanese larch, abundant in Hokkaido, was focused. Japanese larch timber is mainly processed for general timber market and for paper industry as pulp. Pictures of a forest and discarded wood conditions of Japanese larch are shown in Fig. 1. They were taken in Engaru, local town in Hokkaido, at the time when the National and Private Forests Meeting was held in this area.

The Stylus TG-630 camera (Olympus Tokyo, Japan) was used. Analyses were carried out, using the Image J and IrfanView.

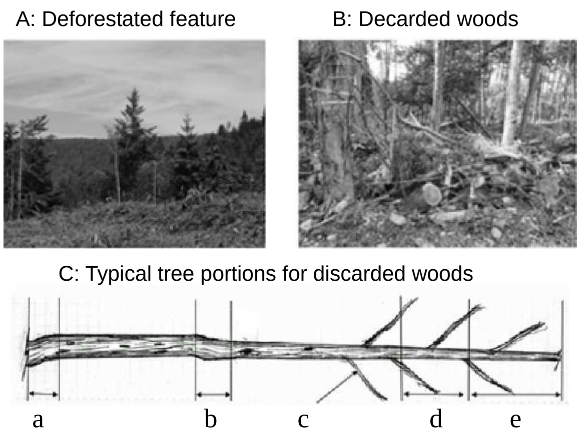

a) warped wood shaft nearby ground, b) twisted part in the middle of shaft, c) bough, d) slender shaft unusable for pulp, e) thin shaft up to crown and twig

Fig. 1 Japanese larch in Hokkaido (modified illustrations via Official Website of Hokkaido Prefecture, 2018c)

Calorific assessment is crucial for each available wood chip for boilers. There remain a variety of arguments on standardization of calorific assessment of wood chips for even wood-burning stoves. Actual calories of burning wood fuels are dependent on the moisture content of them, and on various factors, such as wood materials themselves, boilers and structures of power plants, including the storage conditions.

In this paper, the author decided to choose the calculation method available at the web site of Japan Woodchip Manufacture's Association 2018. The calculation scheme, originally for cone calorimeter, is on the base of perfectly dry wood conditions, although the moisture contains in actual wood fuels even at the furnace to some extent.

The fraction of the evaporable moisture /water content of the wood fuels designated by U_w, is simply given by

$$U_w = (W - W_0) / W \times 100 \qquad \text{in \%} \qquad (1)$$

where W_0 is the mass of the wood fuel in perfectly dried conditions and W is the mass of the one in actual conditions. Heat potential estimations were carried out for actually available wood chips, applying the simple formula (1).

3.2 Market prices of timber and fuel oil

Monthly average timber prices are available on the Min-yurin Shimbun, timber market newspaper in Japan. As to the both of fuel prices, the actually paid prices by the City of Mombetsu were adopted in this study.

These prices are key factors on this theme. There had been a few discussion papers published on the prices before (Yoda and others, 2010, 2011, 2012a and 2012b; Vesergaard, and others, 2011a and 2011b; Chahal and others, 2011; Phan and others, 2013; Yoda and others, 2017). The experience led to adopt the abovementioned price system.

4.Results and Discussion

The trees in Hokkaido have reportedly around 4,000 - 5,000 kcal/kg. The heat potentials of several kinds of wood are available in various reports. Fig. 2 shows one of them (Official Website of Japan Woodchip Manufacturers' Association, 2018). Those data were obtained by use of a cone calorie meter in completely dry conditions.

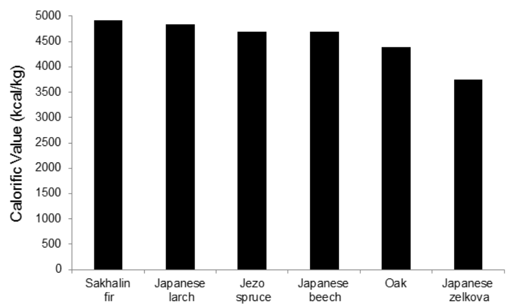

Fig. 2 Calorific values of several kinds of tree

The calorific values of trees in the ideal moisture conditions were found of a little difference among the kinds of tree.

It has been empirically well known that the heat potentials of wood or wood chips are dependent on the moisture or water content in them. The traditional data tell the woods of 20% water content has as much as double calorific value to those of 100% content ones, and the woods within 10-20% water content are ideal for burning for heat generation, while in reality, most of woods for heating have around 30% water content, except for extreme cases.

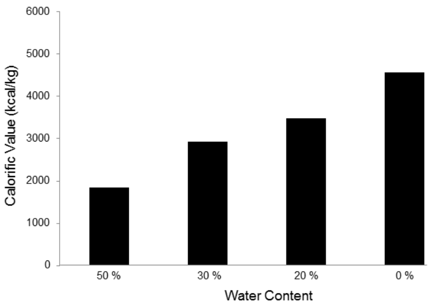

Fig. 3 Calorific values of a wood in different water content conditions

Calorific values in the different moisture conditions were obtained by collecting and analyzing those open web data, as shown in Fig.3.

There has been no reliable data about the water/moisture contents of each portion of discarded wood which is kept in the same natural conditions. Boughs and twigs would have rapid responses to the change of ambient moisture content, that is to say, in rainy days or in dry and windy days. Together with this, heat mass volume of boughs and twigs is minor in biomass heating and wood chips are usually stored in open enclosures.

Taking account of these, in practice, the heat potential of biomass wood chips would be assumed to be the value of the market timber approximately, probably without choice, particularly in the case of feasibility study of wood chips for biomass heating. Fig. 3 suggests that the wood chips could have the heat potential of 3,000 kcal/kg, while fuel oil has 9,600 kcal/kg in the EU industry.

The price trends of biomass wood and the price of fuel oil, as a strong competitor in energy market, form the staple of the total cost. Monthly timber price trends are available in the Min-yurin Shimbun in 2015.

The wood chip price market was found stable through the year. The wood chips of broad-leaf trees have the highest price, and a notable difference exists in the prices between the wood chips of broad-leaf and the others.

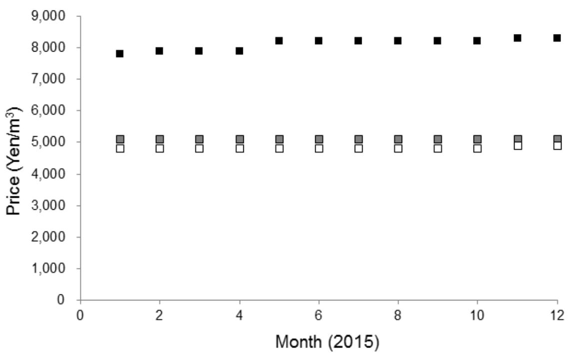

Fig. 4 Monthly price trends of discarded woods. Broad-leaf trees (back squares in the figure), Yezo spruce and Sakhalin fir (grey squares), and Japanese larch (white squares).

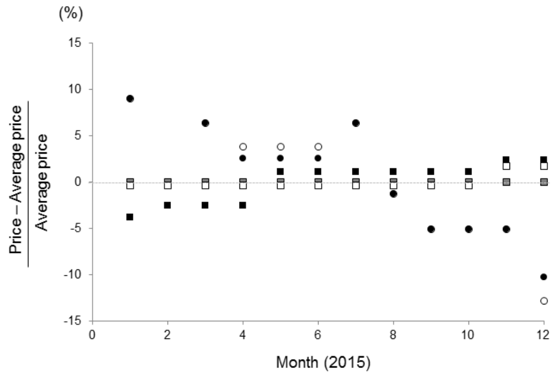

Fig. 5 Monthly oil and wood chips price deviations. Deviations in price of heating oil (black circles), those of fuel oil (white circles), and those of wood chips. Squares are as same as in Fig.4.

Monthly fuel oil price and wood chip price deviations are shown in Fig.5. The oil price varied throughout the year and its trend was of typical ones in the regions cold in winter and warm in summer. However, it should note that the recent oil price trends have been affected by the global markets and international political policies.

As far as the timber market concerns, the price of broad-leaf timber was the highest among these three kinds through the year. The Japanese larch was the cheapest. The prices of both Sakhalin fir and Japanese larch had similar trends.

Discarded wood for power plants has advantages in cost and emission, although another advantage, which will accrue to much better circumstances for reforestation, has been never recognized in those prices.

The disadvantages of the discarded wood chips lye with their thermal qualities, in particular, water contents; depending on the portions of trees while discarded, and natural conditions during the storage.

Especially in Hokkaido, winter season with snowing lasts six or seven months. The discarded wood chips are kept in wet conditions for a long time.

Drying discarded wood chips will be technically easy, but it requires the energy for drying and closed storage rooms, likely bunkers. Such additional, relatively high, expenditures of energy, equipment and facility do not meet the market principle.

The combustion of wood fuels in boilers requires the invariance of the thermal quality of them to generate the maximum efficiency in combustion by easy control. Conversely, boilers need a high capability where fuels of various thermal qualities are stoked up at random into the furnaces, and shall meet the safety regulations at the same time. Eventually, such boilers are slightly more expensive than pellet fueling boilers, where burning dry and nearly homogeneous wood fuels and being easily controlled, and much more expensive that oil fueling boilers.

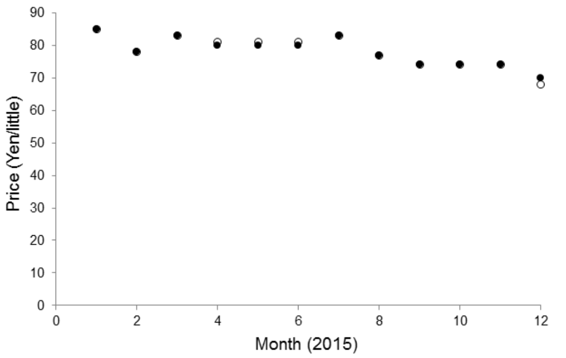

Fig. 6 Price trends of wood and oil fuel. These are actual prices for both heating oil (black dots) and fuel oil (white dots).

The prices in Fig.6 are those of actually paid by the city of Mombetsu. Fig. 6 suggests, to protect biomass industry, the city had controlled the price of biomass wood.

The price of 300kW biomass boiler is around 30 – 40 million yen in Hokkaido, while in Europe the similar boilers are available at the price of about 5 million yen.

The other disadvantage lies with the process of discarded wood chips from forest to power plant. The high processing cost of them consequent the wood chips had been discarded in forest until the time of reforestation.

The author obtained the data as high as 10,000 yen/m^3 for the processing cost estimations from several companies. The cost should be added to the total cost of biomass power plant. Biomass power plant using wood chips as basic fuels would hardly survive under such high cost structure.

To find and examine another relatively cheap wood material had naturally been carried out to solve this cost problem. They were by-products and residues from wood processing industry (BPS in brief). The author obtained the market price of those wood materials around 1,000 – 3,500 yen/m^3.

A previous study derived the conclusion by cost simulations: when the price of BPS in market hovers around or goes over 3,605 yen/m^3, the profit of biomass power plant would be likely to accrue (Nakama and others, 2011). The study also estimated the possible highest price about 6,800 yen/m^3.

The price of BPS materials were lower than those of discarded wood. In case of the unusable timber chips as the base fuel materials for boilers, the total cost for generation of heat or energy would be considerably reduced. However, a question arises; whether the timber industry could provide the amount of such materials enough to stable use for the boilers as its base fuel. In practice, the wood fuels for power plant would be blends and mixtures of discarded wood and BPS chips. Another problem still remains; the cost of boilers for them, in comparison to oil fueling boilers.

If wood fueling boilers are working well for a long time, without serious slagging and fouling problems, the difference at initial investment could be collected through the operations over 15 years due to low price of fueling wood.

As beforementioned, under the new government energy policy to reduce carbon emission, local governments have been demanded to use the discarded wood for heating units and power plants, where those biomass materials could be available. Local governments such as the city of Mombetsu had established the subsidy scheme for the discarded wood, mainly for its processing expenditures. The city of Mombetsu, for instance, has granted 300yen/m^3 subsidy to utilizations of unusable timber materials for the biomass power plant.

The Hokkaido Prefectures grant the subsidies for the acquisition of boilers burning unusable wood materials and other necessary facilities (Official Website of Hokkaido Prefecture, 2018d). The similar subsidies afforded the city of Mombetsu to support a hospital management where biomass boilers are working for heating system.

Enlargement efforts of the local consumer’s market would contribute further reduction of the cost as well as total amount of carbon emission, where the role of proximity dimensions in facilitating biomass power plants should be demanded.

5.Conclusion

The economic aspects are always key issues in biomass energy. Putting stress on it, the author studied the biomass fuels for heating units and power plants, discussing their present state and future prospective, in a local city in Hokkaido. There are several problems left in the effective use of biomass materials. To solve them, the local governments together with the local communities will have to assume the executive responsibilities on the biomass issues.

Since we can no longer leave the nature to manage itself under our onslaught, changing the discarded or wasted materials to be useful energy resources could be one step forward to realize the healthy nature again as well as sustainable human society.

Acknowledgements

The author is grateful to Mr. Shuichi Tokusho, a manager in the biomass section of the city of Mombetsu for his warm support. The author would like to extend the author’s deepest thanks to the reviewer for his painstaking reviewing work.

References

Bateman I.J., G.M. Mace and 3 and others (2011) Economic Analysis for Ecosystem Service Assessments. *Environ. Resource. Econ.* **48**:177-218.

Chahal B, M.C. Vestergaard and 3 others (2011) Structure-dependent membrane interaction and bioactivity of flavonoids with lipid bilayers., *Micro-Nanomechatronics and Human Science (MHS), 2011 International Symposium* 451-455.

FAOSAT (2016) Annual Report on Forest and Forestry in Japan; 34.

Government of Japan (2009) Fundamental Law of Promoting Usage of Biomass, Act No.52, enacted 2009 (in Japanese).

Government of Japan (Cabinet) (2010) Basic Plan for the Promotion of Biomass Utilization, (in Japanese).

Government of Japan (Cabinet) (2016) Basic Plan for Promotion of Biomass Utilization, (in Japanese).

Government of Japan (2017) Act on Promotion of Use and Distribution of Legally-harvested Wood and Wood- Products (Clean Wood Act), 13.

Kuboyama H, T. Nishizono, T Iehara, H. Okuda (2004) Feasibility of Wood-biomass Utilization as an Energy Source: Case Study in Tohno City, Iwate Prefecture. *J. Jpn. For. Soc.* **86**: 112—420.

Ministry of Agriculture, Forestry and Fisheries (MAFA) (2012) Annual Report on Forest and Forestry in Japan (in Japanese)

Ministry of Economy, Trade and Industry of Japan (METI) (2012) Feed-in Tariff Scheme in Japan, 36.

Nakama K., T. Ota, N. Mizoue, S. Yoshida (2011) Effects of recovering logging residues on strategy and benefits of forest stand management. *J. Jpn. For. Soc.* 93: 226-234.

Niseko's Towns efforts as an Eco Model City (2018) [online] http://futuecity.jp/pdf/forum/2015_malaysia/Case/Study_of_Japan_01_06_01_Town_of_Niseko.pdf

Official Website of Japan Woodchip Manufactures' Association (2018) [online]http://zmchip.com/houkoku232.pdf (Accessed 5 Mar 2018).

Official Website of Hokkaido Prefecture (2018a) [online]http://www.okhotsk.pref.hokkaido.lg.jp/ss/rnn/biomas /kouminkan.pdf (Accessed 5 Mar 2018).

Official Website of Hokkaido Prefecture (2018b) [online] http: //www.okhotsk. pref.hokkaido.lg.jp/ss/ biomass/ kouminkan.pdf (Accessed 5 Mar 2018).

Official Website of Hokkaido Prefecture (2018c) [online] http://www.pref.hokkaido.lg.jp/sr/srk/grp/03/sigendoukoukekka siryou3.pdf (Accessed 5 Mar 2018).

Official Website of Hokkaido Prefecture (2018d) [online] http://www.pref.hokkaido.lg.jp/ks/jss/recycle_2/H23itirann. pdf (Accessed 5 Mar 2018).

Official Website of Hokkaido Prefecture (2018e) [online] http://www.pref.hokkaido.lg.jp/ks/tot/gnd/saienekeiakuH25H26.pdf (Accessed 5 Mar 2018).

Phan HTT, T. Hata and 5 others (2013) The effect of Oxysterols on the interaction of Alzheimer's amyloid beta with model membranes. *Biochim. Biophys. Acta. (BBA)-Biomembr.* **1828**: 2487-2495.

Saidur R, E.A. Abdelaziz and others. (2011). A review on biomass as a fuel for boilers. *Renew.Sustain.Energy.Rev.* **15** (5): 2262-2289.

Vestergaard M.C., T. Yoda and 4 and others (2011) The effect oxycholesterols on thermo-induced membrane dynamics. *Biochim. Biophys. Acta (BBA)- Biomembr.* **1808**: 2245-2251.

Vestergaard MC, T. Yoda and 4 and others (2011) Thermo responsiveness of autooxidized cholesterol-containing lipid membranes, observed in real-time. *Micro Nano Mechatronics and Human Science (MHS), 2011 International Symposium*, 451-455.

Yamamoto Y, K. Takeuchi, T. Shinkuma (2014) Is there a price premium for certified wood? Empirical evidence from log auction data in Japan. *For. Policy. Econ.* **38**: 168-172.

Yoda T (2017) The influx of temporary visitors and lodgers to Mombetsu City for construction projects: a quantitative study of the period between 2009 and 2014 *Int. J. Knowl. Manag. Tour. Hosp*, **1**: 477-488.

Yoda T, M.C. Mun' delanji and 3 others (2012a) Thermo-induced vesicular dynamics of membranes containing cholesterol derivatives. *Lipids*, **47**: 813-820.

Yoda T, H.T.T. Phan and 3 others (2012b) Thermo-induced dynamics of membranes and liquid crystals containing cholesterol derivatives. *Micro-Nano Mechatronics and Human Science (MHS), 2012 International Symposium*, 87-92.

Yoda T, M. C. Vestergaard and 4 others (2010) Dynamic response of a cholesterol-containing model membrane to oxidative stress. *Chem. Lett.* **39**: 1273-1274.

Okhotsk Sea and Polar Oceans Research 3 (2019) 13-19

Article

Turning features of an icebreaker during ramming operations: a case study

Yuto TAKAHASHI[1], Hajime YAMAGUCHI[1], Shuki USHIO[2],
Yutaka YAMAUCHI[3] and Shigeya MIZUNO[3]

[1] *Graduate School of Frontier Sciences, The University of Tokyo, Kashiwa, Japan*
[2] *Meteorology and Glaciology Group, National Institute of Polar Research, Tachikawa, Japan*
[3] *Technical Research Center, Japan Marine United Corporation, Tsu, Japan*

(Received September 30, 2018; Revised manuscript accepted December 25, 2018)

Abstract

Syowa Station, Japan's main Antarctic research base, is located in Lützow–Holm Bay (LHB) This bay is often covered with very thick multiyear landfast ice. The Japanese Antarctic research icebreaker *Shirase II* conducts "ramming" icebreaking operations comprising repeating backing and ramming, sometimes thousands of times, in one cruise. In this study, we analyzed data for turning in ice while ramming, which is a rare occurrence. The turning angle per ramming procedure and the turning radius are correlated with the ramming penetration distance. Thus, the required time and ice area width for one turn can be estimated from the data of the first several ramming trials. In addition, shortening the approach run length decreases the time required per ramming procedure and the turning trajectory and increases the required number of ramming procedures. To balance these effects, we attempted to reduce the total required time by controlling the approach run length. It was concluded that the best operation to reduce the turning time is to use an approach run length that is sufficient to achieve high impact velocity, unless the brash ice in the broken channel significantly prevents the ship's astern movement.

Key words: icebreaker, ramming, turning, maneuverability, navigation support

1. Introduction

Syowa Station, Japan's main Antarctic research base, is located in Lützow–Holm Bay (LHB). This bay is often covered with very thick multiyear landfast ice. While icebreakers can usually navigate with continuous icebreaking, the ramming operations (i.e., backing and ramming) are required in areas where the ice thickness exceeds a certain level. In this operation, an icebreaker repeats the following procedure:

1. Move astern for an approach run
2. Accelerate using a channel (made by the previous ramming operation) and impact on ice at high speed
3. Penetrate using kinetic energy and propulsion thrust

This procedure requires significant time and fuel. In LHB, the Japanese Antarctic research icebreaker *Shirase II* (hereafter called *Shirase*) sometimes conducts thousands of ramming operations in one cruise.

During navigation under very heavy ice conditions, icebreakers sometimes need to turn during ramming operations. *Shirase* has made 180° turns during ramming operations in both the 2012/2013 and 2017/2018 cruises. Turning by 180° during ramming operations can require half a day or more, so its efficient execution is important.

Many studies (e.g., Daley and Riska, 1990) have investigated straightforward ramming performance. By contrast, only some studies (e.g., Nozawa, 2006) have investigated turning performance with continuous icebreaking, and little is known about turning ramming performance because this operation occurs rarely.

Owing to the low frequency of turning ramming operations, valuable data can be obtained from multiple turns with ramming by the same icebreaker. In this study, we investigate the turning of *Shirase* to determine principles for conducting more efficient turning and to provide information for navigation planning.

2. Method

Table 1 lists the main dimensions of *Shirase* (for other specifications, refer to Yamauchi and Mizuno, 2009). *Shirase*'s navigation data is recorded using a ship-monitoring system (SMS) that records basic navigation information including GPS location (accuracy: < 10 m), ship motion, steering angle, and engine power (Yamauchi et al., 2011). Navigation data of four turns from the last nine years are extracted analysis (Table 2). The ice thickness values (h) observed during the turns are shown in the table only as guides; they are roughly estimated by image analysis of photos taken with a compact digital camera (2012/2013) and by unaided visual observation (2017/2018). Slash-delimited numbers indicate observed samples. Image analysis is conducted based on the same principle as the video method conducted since 1988 (Shimoda et al., 1997). However, it is considered less accurate than the video method because the compact camera was not fixed, which may have caused large variations in observed values. Although the ice thickness may vary during a turn, we did not consider this in this study because of the lack of high-precision data with high sampling density.

The inner part of LHB contains “landfast level ice” (Turns 1–3) of high and stable thickness. Furthermore, “Hummock ice” of variable thickness develops on the ice edge.

Table 1. Main dimensions of *Shirase* (Yamauchi and Mizuno, 2009)

Overall length	138.0 m
Length of water line	126.0 m
Maximum breadth	28.0 m
Depth	15.9 m

Table 2. General descriptions of analyzed turns

	Season	Ice feature	Ice thickness (m)
Turn 1	January, 2013	Landfast level ice	2.6 / 4.0
Turn 2	February, 2013	Landfast level ice	4.2 / 4.4 / 5.2
Turn 3	January, 2018	Landfast level ice	1.7 / 2.1
Turn 4	February, 2018	Hummock ice near ice edge	2.1 / 2.2

The navigation data is analyzed through the three steps described below.

1) Ramming section extraction and characteristic parameter calculation for each ramming procedure

In this study, one ramming procedure is defined from starting astern movement to stopping the ship body after penetrating the ice. Fig. 1 shows an example of a ramming procedure extracted from SMS data. The shaft speed and rudder angle are the average of two values. A ramming procedure is decomposed into three phases:

A) Astern

This phase is defined from stopping the previous ramming procedure to starting the next approach run, including a few minutes for reversing the engine rotation. The ship speed is controlled carefully to avoid collisions with the ice, typically by changing the shaft speed at a rate <120 rpm to maintain a velocity of <1.5 m/s. The rudder is kept neutral during astern movement to avoid damage, and the traveling direction is controlled by changing the balance of the left–right thruster output. For typical ramming navigation of *Shirase*, the astern distance (identical to the approach run length discussed below) is ideally 300 m. The actual astern distance must sometimes be shorter mainly because brash ice fills the channel and reduces the efficiency of astern movement. The astern distance can also be reduced intentionally when ramming partially weak or cracked ice. Such operations are often used with hummock ice.

B) Approach run

After the astern movement phase, the ship accelerates with high engine power through the channel. In the present analysis, *Shirase*’s regular operational speed of 137 rpm was used for all but two cases. The rudder angle is controlled to follow the channel shape and then strongly turned in the direction of turning so that the ship collides with the side of the previous ramming print, which has a curvilinear triangular shape.

C) Penetration

After colliding with the ice edge, the ship penetrates the ice under high engine power. The rudder is kept neutral or at a small angle to reduce water resistance. This phase is defined as ended when the ship is at a complete stop for 5 s.

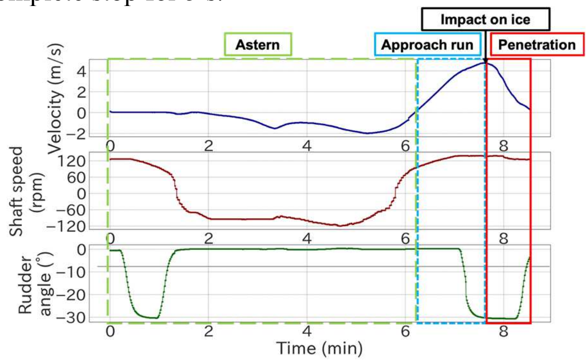

Fig. 1 Typical change of velocity, engine power, and rudder angle during ramming

First, we define the impact velocity (V). Because the exact time at which the ship impacts ice is difficult to identify, in this study, we assume that the velocity is maximized when the ship impacts ice. Thus, the impact velocity is defined as the maximum speed during each ramming procedure. Vance (1980) noted that the impact velocity increases with the approach run length (L) although it reaches a specific impact velocity with a sufficient approach run length. Through field experiments with the *USCGC Katmai Bay* icebreaker, Vance (1980) also suggested that the impact velocity converged to its maximum after accelerating for 2.5–3.0 ship lengths. For *Shirase*, the impact velocity is controlled at <5–6 m/s to maintain sufficiently low ice pressure on the ship hull. The approach run length needed to achieve this impact velocity is 300–400 m, that is, 2.5–3.0 ship lengths.

Second, we define the penetration distance (D) as the distance between the impact point and the ship stopping point. This variable is often used to indicate ramming progress on site. The penetration distance varies with the ice condition and impact velocity.

The turning angle (Θ) is defined as the difference in heading between the first and the last ramming procedure during a turn. It represents the total displacement angle of the turn; it varies between cases because the selected turns do not necessarily reach 180°. N denotes the required number of ramming procedures, and the turning angle per ramming procedure (θ) is calculated as Θ/N.

2) Projection of ramming positions to *X*–*Y* plane

The GPS position of the ship stopping point for each ramming procedure is extracted from the above ramming datasets and projected to the *X*–*Y* plane. The longitude and latitude are taken as the *X*- and *Y*-axis directions, respectively, with north and east being positive.

3) Calculation of turning circle and its radius

The turning circle is approximated by nonlinear least-squares fitting as the trajectory of each turn. Its radius is calculated and defined as the turning radius (r). Although the trajectory of a continuous icebreaking turn is rarely a geometrical circle, we assume it to be a geometrical circle for ramming turns.

3. Results and discussion

3.1 Turning features

Table 3 shows the statistics of each turn. The ramming positions and fitted circles are plotted concentrically in Fig. 2. The subscript *av* denotes the averaged values for the turn.

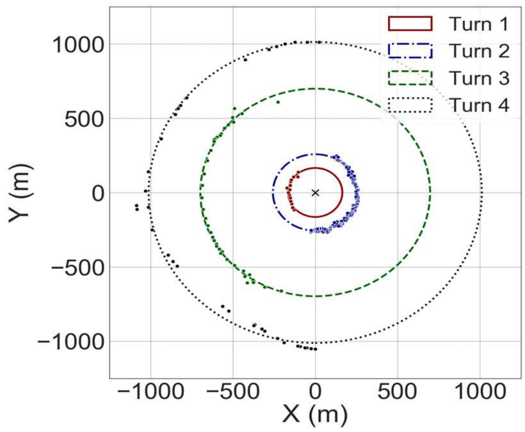

Fig. 2 Concentric plot of ramming endpoints and fitted circles for four turns

Table 3. Statistics of four ramming turns

	N	r (m)	V_{av} (m/s)	D_{av} (m)	L_{av} (m)	Θ (deg)	θ (deg)	h (m)
Turn 1	15	164.7	7.3	104	264	52	3.4	2.6 / 4.0
Turn 2	143	257.2	6.6	52	158	158	1.1	4.2 / 4.4 / 5.2
Turn 3	39	697.9	9.0	118	292	142	3.6	1.7 / 2.1
Turn 4	35	1012.3	6.6	143	201	179	5.1	2.1 / 2.2

Table 4 Maneuverability test results with continuous icebreaking (analyzed by the University of Tokyo, not published)

	Season	Estimated radius (m)	Ice / snow thickness (m)	Velocity (m/s)	Engine power (rpm)	Rudder angle (deg)
Exp. 1	December, 2009	560	0.7~1.0 / 0.3	4~4.5	137	30 (partially 15)
Exp. 2	February, 2010	760	0.3~0.5 / 0	2~4	95	30

The turning radii clearly vary. For two experiments conducted in 2009/2010, the turning radii during continuous icebreaking were 560 and 760 m, respectively (Table 4). The present study shows that the turning radius during ramming sometimes becomes smaller than that during continuous icebreaking.

Fig. 3 shows the quantitative relation between D and r. The turning radius increases with the penetration distance. The figure shows the regression formula and its correlation coefficient R. Despite the low number of samples, it is expected that the turning radius for an area can be roughly estimated by conducting several ramming procedures and calculating their penetration distances.

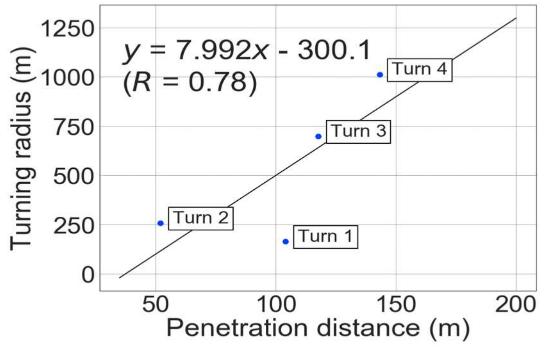

Fig. 3 Relation between penetration distance (D) and turning radius (r)

Because thicker ice reduces the penetration distance, the turning radius decreases with increasing ice thickness. However, Nozawa (2006) noted that the turning radius with continuous icebreaking increases as a function of ice thickness. The results of the present study are not consistent with this previous report. Here, we discuss the reason for this inconsistency by focusing on the unique features of ramming.

All ramming tracks of Turns 2 and 3 are plotted in Fig. 4 in different colors. The GPS data during penetration only are plotted. This shows that each ramming track is a nearly straight line throughout the turn. In particular, 20 and 10 consecutive ramming examples are extracted from Turns 2 and 3, respectively, and plotted in Fig. 5. This shows that during penetration, the tracks are like straight lines with slight changes in heading angle, although slightly curved tracks are seen in Turn 3.

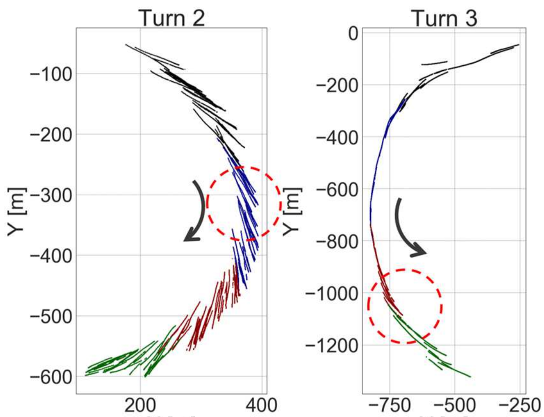

Fig. 4 Tracks during penetration. Red dashed-line circles denote extracted areas shown in Fig. 5.

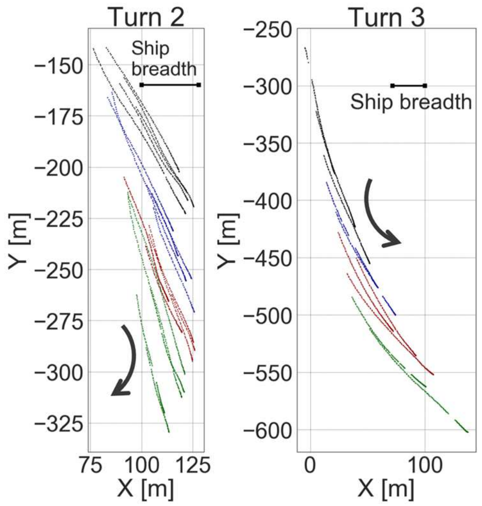

Fig. 5 Tracks during penetration (20 and 10 consecutive ramming procedures from Fig. 4 extracted for magnification.)

The relationship shown in Fig. 3 can be explained as follows. The turning angle is mainly achieved during the approach run and less so, if at all, during penetration. Therefore, longer penetration distances expand the tracks outward, thereby lengthening the turning radius compared to that in gradual (short penetration distance) ramming.

If this holds under all conditions, it is possible that the longer penetration distance does not contribute to the efficiency of a ramming turn. In fact, gradual ramming with shorter penetration distances may be more efficient because of the shorter trajectory. It is critical to determine whether the turning angle is achieved to any extent during penetration.

To discuss this more quantitatively, the time series data of the ship's yaw rate and velocity are shown in Fig. 6. Each line represents each turn, as obtained by averaging each ramming procedure after aligning the procedures such that the impact timing on the ice is 0 s. The turning direction is considered positive for the yaw rate plot of each turn. The yaw rate is clearly maximized during the approach run, and it decreases rapidly after impact. This is attributed to the ship bouncing from the ice edge. The yaw rates of Turns 3 and 4, which have long penetration distances, remain positive for a while. Although the yaw rate does not necessarily coincide with the angle of the navigation track, it implies that some of the turning angle can be achieved during the penetration phase. However, the amount is smaller than that during acceleration, such that the turning radius is increased, as in the discussion following Fig. 5.

For greater clarity, the turning angle per ramming procedure θ is calculated for each turn by dividing the total change in angle by the number of ramming procedures. The result is shown in Fig. 7, with the penetration distance plotted on the horizontal axis.

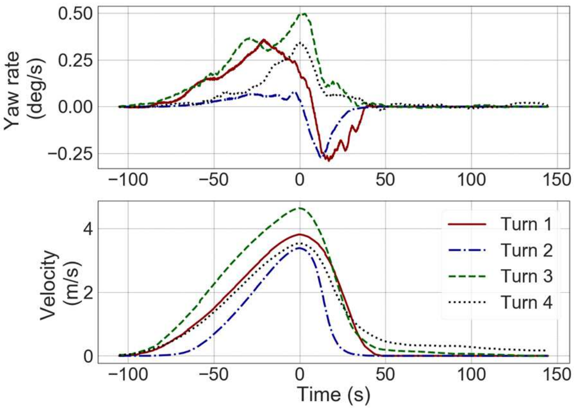

Fig. 6 Averaged yaw rate change and velocity change during ramming for each turn

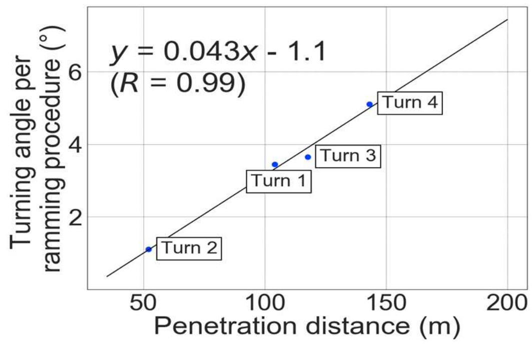

Fig. 7 Relation between penetration distance (D) and turning radius per ramming procedure (θ)

The result shows a clear positive near-linear correlation between the penetration distance and the turning angle per ramming procedure. It can be expected that the required number of ramming procedures to achieve a certain change in angle can be estimated from the penetration distances of several ramming trials, thus yielding the total time required for turning. Because the penetration distance can be observed and calculated easily on site and in real time, this is considered useful for navigation planning.

3.2 Discussions on efficient turning

Next, we attempted to improve the efficiency of the turning operation based on the above results. The conceptual diagram is shown in Fig. 8.

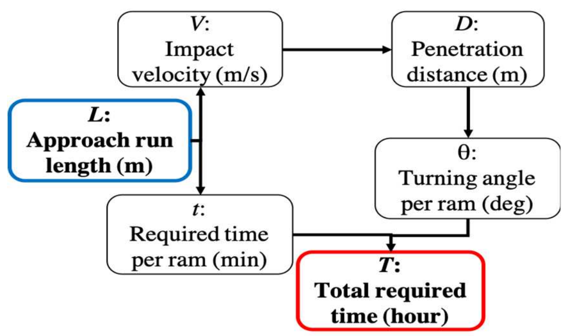

Fig. 8 Conceptual diagram of calculation

The approach run length (L) is chosen as the predictor variable. The navigation officer can control this easily by changing the timing to stop the astern movement. The total required time (T) is defined as the total time required for turning by a certain angle, which is the objective variable to reduce. When we consider a turn of Θ, T can be decomposed into the following equations:

$$T = (\Theta/\theta) \cdot t \qquad (1)$$
$$\theta = a_\theta \cdot D + b_\theta \qquad (2)$$
$$D = a_D \cdot V + b_D \qquad (3)$$
$$V = a_V \cdot L + b_V \qquad (4)$$
$$t = a_t \cdot L + b_t \qquad (5)$$

Therefore, T can be expressed as an equation of only one variable L:

$$T = \frac{\Theta \cdot (a_t \cdot L + b_t)}{a_\theta \cdot (a_D \cdot (a_V \cdot L + b_V) + b_D) + b_\theta} \qquad (6)$$

Here, a and b with subscripts denote constants, and t is the time required per ramming procedure during the turn. Tatinclaux (1992) noted that the penetration distance D is a linear function of the impact velocity V, although the relational expression varies for different ice conditions. The coefficients of the relational expression are calculated for the four areas of turning, as shown in Fig. 9. At this time, it is difficult to identify a tendency between the ice conditions and the features of the regression lines.

We assumed that the dependency of θ on V can be calculated from the relations shown in Fig. 7 and Fig. 9. Though the above discussion indicates that changes in V affect D and thus θ, it is also possible that this effect is small and that the relation shown in Fig. 7 is largely due to the effects of ice condition differences on both D and θ separately. For an accurate calculation, the contribution of V to θ should be quantified without ice condition differences. Because of the shortage of data for such quantification, we assumed that the regression formula shown in Fig. 7 is applicable to the change in D accompanying the change in V. Considering this uncertainty, we calculated seven scenarios: relational expression of the original regression line, 20% raised/inclined, 10% (of average of four turns) parallel upward/downward shifted, and 20% increased/decreased uniformly (Fig. 12).

V and t change depending on L. The relation among V, t, and L is calculated in the same manner as above. Preceding icebreaking tests of *Shirase* (2010/2011, result not published) suggested that the relation between L and V was linear and that the relational expression did not vary significantly for different ice conditions. This is justified because the icebreaker passes an open water channel during the approach run. The results of the present analysis agree with this report, as shown in Fig. 10. However, the correlation between L and t varies for the four turns (Fig. 11). This is attributed to effects on the relation by brash ice coverage in the channel generated by the icebreaker itself. The quantity of produced brash ice is greater in thicker ice areas (i.e., Turns 1 and 2). If the brash ice in the channel is increased, the ice resistance is increased, and thus, the required time per unit length astern distance is longer. Therefore, it is reasonable that the regression lines of Turns 1 and 2 (thicker ice areas) are steeper than those of Turns 3 and 4 (thinner ice areas).

In the regression analyses, some irregular ramming procedures are removed:

1) Extreme penetration distances despite low impact velocities

Two ramming procedures with penetration distances >200 m are removed from Turn 3. Such ramming procedures can be caused by partially thin ice, though the actual cause has not been identified.

2) Low engine power

Two ramming procedures are performed at low velocity because low engine power is used.

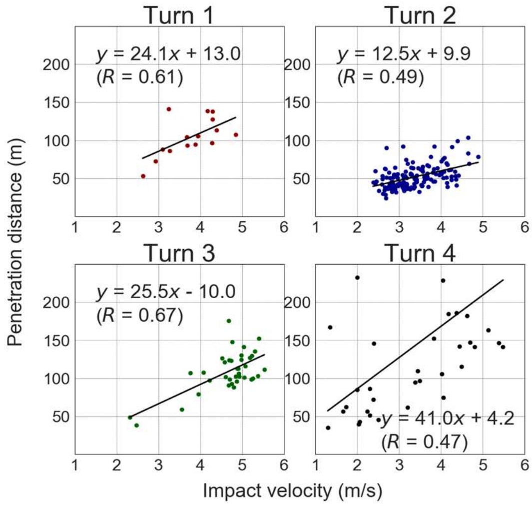

Fig. 9 Regression analysis between impact velocity (V) and penetration distance (D)

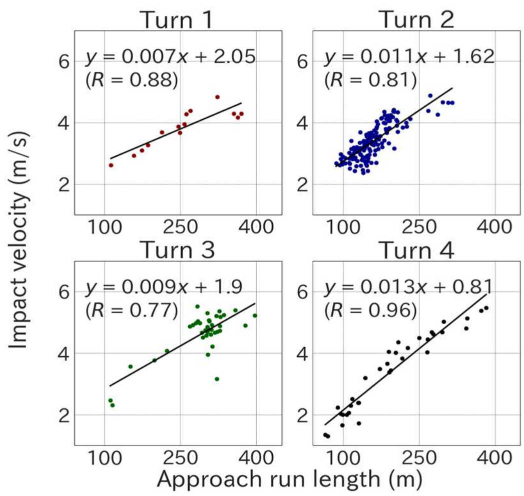

Fig. 10 Regression analysis between approach run length (L) and impact velocity (V)

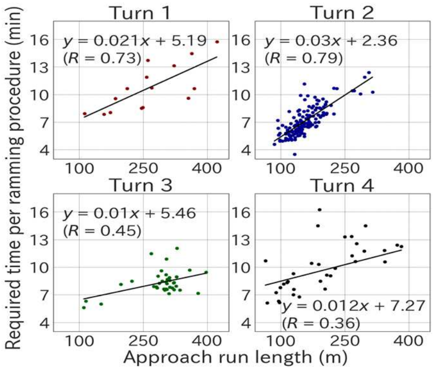

Fig. 11 Regression analysis between approach run length (L) and required time per ramming procedure (t)

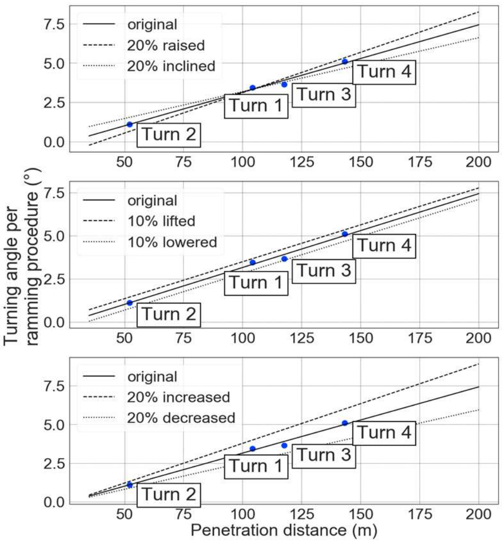

Fig. 12 Relational expressions of seven scenarios between penetration distance (D) and turning angle per ramming procedure (θ)

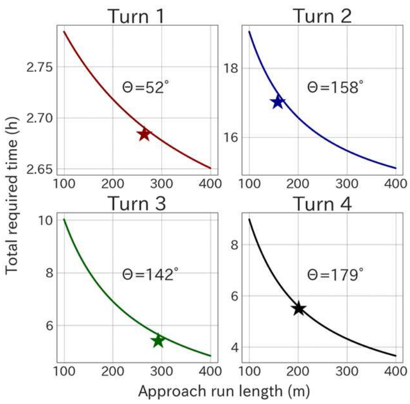

Fig. 13 Estimated total required time (T) and its dependency on approach run length (L). Actual time–length point for each turn is indicated by a star.

By using the relational expressions mentioned above, T is calculated for various L values in the feasible range of 100–400 m. The results are shown in Fig. 13 and Fig. 14. These estimations are compared to the actual required times and averaged approach run lengths.

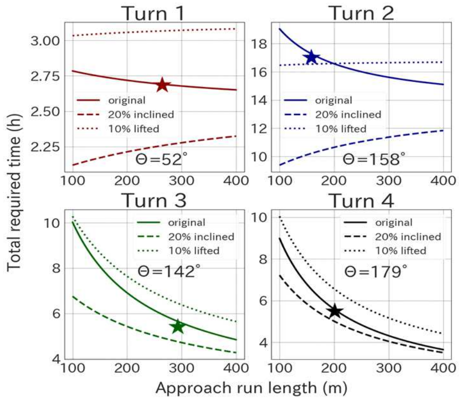

Fig. 14 Estimated total required time (T) and its dependency on approach run length (L) – scenarios of 20% inclined/10% lifted (parallel upward shift) from the original D–θ equation. Actual L–T values are indicated using stars.

In the scenario with the original D–θ regression lines (Fig. 13), T decreases monotonically with L for all four cases. The actual data lies almost on the lines, indicating the reliability of the calculation scheme. The result implies that the approach run length should be increased for a time-efficient turn.

However, Fig. 14 shows that the L–T correlations for Turns 1 and 2 change from negative to positive in two scenarios whereas for Turns 3 and 4, they are negative for all three scenarios. The scenarios not plotted in this figure are all decreasing functions. The reason for this is explained below.

The conditional expression for T as a decreasing function of L is

$$\frac{dT}{dL} \le 0 \qquad (7.1)$$

By calculating this using equation (6), we obtain:

$$-a_D\, a_V\, a_\theta\, b_t + a_t\, b_\theta + a_D\, a_t\, a_\theta\, b_V + a_t\, a_\theta\, b_D \le 0 \qquad (7.2)$$

Here, we conducted a sensitivity study as follows:

1) The average and standard deviation of each coefficient were calculated for the four turns. For a_θ and b_θ, the value itself is used for the mean value and 50% of its value is substituted for the standard deviation as a guide.
2) The standard value is calculated by substituting the averaged coefficients into the left-hand side of (7.2).
3) Each coefficient is increased by its standard deviation while holding the others constant, and the difference from the standard value is calculated for each coefficient (hereafter defined as sensitivity).

The results are shown in Table 5. It shows that b_t has the greatest influence compared to the other coefficients. This suggests that the L–t relation has the greatest contribution to the shape of the L–T curve. Here, we must consider that b_t changes depending on

a_t in the process of regression analysis. This complication arises because the linear model assumption is not applicable for small values of L (< 100). Theoretically, t at L = 0 should be constant regardless of ice conditions.

Based on the above discussion, the results shown in Fig. 14 can be explained as follows. In Turns 1 and 2, heavy ice conditions yield regression lines with larger a_t and smaller b_t (see discussion on page 17), thus making *dT/dL* positive.

Table 5 Sensitivity of *dT/dL* to each coefficient

a_t	b_t	a_V	b_V	a_D	b_D	a_θ	b_θ
0.01	-11.36	0.00	-0.28	-0.13	0.21	0.00	-0.02

These results suggest that the approach run length should be lengthened for time-efficient turns, especially when brash ice coverage in the channel is low and the approach run length can be increased relatively freely. However, this does not always apply if brash ice fills the channel.

For predicting the total required time, Fig. 13 and Fig. 14 show that the total time changes by up to 50% depending on the approach run length. Again, if the brash ice prevents a long approach run, the turn may require more time than that predicted using the relation shown in Fig. 7. Further studies are required for the practical prediction of the total required time for turning while ramming.

4. Conclusions

The turning performance under ramming operation is investigated by analyzing data from four turns conducted in actual ice-covered sea. As a result, the following features of ramming turns are obtained:

- The turning radius increases almost linearly with penetration distance.
- The turning angle per ramming procedure increases with the penetration distance despite the longer trajectory.
- The total required time for turning decreases with increasing approach run length for 100–400 m runs, unless brash ice significantly prevents the ship's astern movement.

Based on these results, the following navigation guidelines for ramming turns are suggested:

- To reduce the turning time, the approach run length should be increased unless brash ice significantly fills the channel.
- For an icebreaker that is forced to turn in a narrow area, it may be effective to shorten the penetration distance to achieve small turns.
- It is expected that the total required time for turning can be estimated using the penetration distances of the first several ramming procedures during a turn, although this method has low reliability based on the results of the present study.

To confirm the validity of the analysis, a field experiment of two turns in one area with varying approach run lengths is desired. In addition, turns performed by other icebreakers must be investigated to generalize the results. It has already been suggested that the turning performance during continuous icebreaking varies depending on the shape of the ship (Nozawa, 2006; Sazonov, 2011).

Acknowledgements

The authors wish to acknowledge support from Japanese Antarctic Research Expeditions (JAREs) and a "Kaken-hi" grant (no. 26249133) from the Japan Society for the Promotion of Science. We also thank the ship crew of JARE 59 for their cooperation. We are also indebted to the Antarctic Research Support Section, Ministry of Defense, for their permission to publish this work. We thank Dr. Ito (Institute of Low Temperature Science, Hokkaido University) for providing ice observation data.

References

Daley, C. G. and K. Riska (1990): *Review of Ship-ice Interaction Mechanics Report from Finnish-Canadian Joint Research Project No.5 "Ship Interaction With1 Actual Ice Conditions" Interim Report on Task 1A*. Helsinki, Finland: Helsinki University of Technology

Nozawa, K. (2006): *Engineering for ice-covered seas*. Tokyo, Japan: Seizando-Shoten Publishing Co., Ltd. (in Japanese)

Sazonov, K. E. (2011): Navigation challenges for large-size ships in ice conditions. *Ship and Offshore Structures*. **6:3**. 231-238. doi: 10.1080/17445302.2010.548123

Shimoda, H., T. Endoh and 6 others (1997): Observation of sea-ice conditions in the Antarctic coastal region using ship-board video cameras. *Nankyoku-Shiryo (Antarctic Record)*. **41(1)**. 355-365. (in Japanese)

Tatinclaux, J. C. (1992): Tests in ice on an Antarctic research vessel model. Retrieved from http://www.dtic.mil/ dtic/tr/ fulltext/u2/a249789.pdf

Vance, G. P. (1980): Analysis of the performance of a 140-foot Great Lakes icebreaker USCGC KATMAI BAY (No. CRREL-80-8). *Cold Regions Research and Engineering lab Hanover NH*.

Yamauchi, Y. and S. Mizuno (2009): Study on improvement in ramming performance of Antarctic icebreaker. *Proc. of the 19th International Offshore and Polar Engineering Conference (ISOPE-2009)* CD-ROM. 629-635.

Yamauchi, Y., S. Mizuno and H. Tsukuda (2011): The icebreaking performance of SHIRASE in the maiden Antarctic voyage. *Proceedings of the 21th International Offshore and Polar Engineering Conference (ISOPE-2011)* CD-ROM. 1093-1099.

Submission Information for OSPOR

Reviewing processes of OSPOR

1) When manuscripts have been received by the Editor-in-Chief, an acknowledgement of receipt will be sent to the author(s) by e-mail. The Editor-in-Chief chooses an editor to handle the manuscript review.
2) The submitted manuscript will be subjected to screening review for its scope, novelty, completeness, English level, and conformation to the OSPOR policy. A manuscript not passing the screening review will immediately be returned to the authors.
3) The editor in charge will select expert reviewers to evaluate the manuscript.
4) As to results of review, if the editor decides that the paper needs revision by the author(s), the manuscript will be returned to the author(s) for revision.
5) Manuscripts returned to author(s) for revision should be resubmitted promptly. If the revision cannot be finished within a month, the manuscript will be regarded as having been withdrawn.
6) The Editor-in-Chief will finally decide whether to accept the manuscript for publication.

Paper Submission

Submission Guideline

All manuscripts should be submitted in digital format (PDF or WORD) with the OSPOR submission sheets (PDF or WORD, offered from OSPOR) by email to the OSPOR Editorial Board

OSPOR Editorial Board

Polar Oceans Research Association (OSPORA)

Address: Kaiyo Koryukan, 1 Kaiyo Koen, Mombetsu, Hokkaido 094-0031 Japan
E-mail: momsys@o-tower.co.jp
Phone : +81-158-26-2810 (Japan 0158-26-2810)
Fax: +81-158-26-2812 (Japan 0158-26-2812)

Publication Charge

Authors of their institutions are requested to pay the publication charge according to the following rate when paper is accepted.
5,000 Yen / (paper)

Copyright

Copyright for an article submitted to OSPOR is transferred to OSPORA when the article is published in OSPOR in any form.

Preparation of manuscripts

The manuscript should be formatted in the form of OSPOR template offered from the OSPORA office, which satisfies the following requirements. The maximum page in printing style is 6 pages.

1) Text
   a) The manuscript should be in the international size A4 in camera-ready style according to the form of OSPOR template.
   b) The first page should include: the title, the author(s) name(s) and their affiliations. If possible, a Japanese translation of the title and the name(s) of the author(s) should be provided in the end of manuscript. If they are not, the translation will be undertaken by the OSPOR editorial board.
   c) An abstract not exceeding 250 words must be provided.
   d) Up to five keywords that describe the content for indexing purposes must be provided.

2) References

a) A list of cited references should be arranged alphabetically. Journal abbreviations are better to use, but when the abbreviation is not known, the full title of the journal should be used in the list.

In the case of many authors, the author name can be written in short as below.

Kawamura, K., F. Parennin and 16 others (2007): Northern hemisphere forcing of climatic cycles in Antarctica over the past 360,000 years. *Nature*, **448**, 912-916.

b) References in the text will include the name(s) of the author(s), followed by the year of publication in parentheses, *e.g.* (Clark, 2003), (Li and Sturm, 2002), (Harrison and others, 2001).

3) Units

Numerical units should conform to the International System (SI).

Units should be in the form as kg m^{-3} not as kg/m^3.

4) Tables

A title and a short explanation should be located on the top of table.

They should be referred to in the text.

5) Figures

a) All Figures (illustrations and photographs) should be numbered consecutively.

b) All Figures should be of good quality and referred to in the text.

c) Figure captions should be located on the bottom of the Figures.

6) More information

For more information about manuscript instruction, please ask to OSPORA office or see OSPORA home page in http://www.o-tower.co.jp/okhsympo/top-index.html.

[Appendix]

PROGRAM of
The 34th International Symposium
on Okhotsk Sea and Polar Oceans, 2019

Date: 18-20 February 2019

Place: Mombetsu Citizens' Public Hall,
Mombetsu Arts & Culture Center,
Mombetsu Municipal Museum,
at Mombetsu, Hokkaido, Japan

Okhotsk Sea and Polar Oceans Research Association
(OSPORA)

Okhotsk Sea and Polar Oceans Research, Vol. 3 (2019, February)

Published by the Okhotsk Sea and Polar Oceans Research Association (OSPORA),
Mombetsu City, Hokkaido, Japan

Address: Kaiyo Koryukan, 1 Kaiyo Koen, Mombetsu, Hokkaido 094-0031 Japan
E-mail: momsys@o-tower.co.jp
Phone : +81-158-26-2810 (Japan 0158-26-2810)
Fax: +81-158-26-2812 (Japan 0158-26-2812)
http://www.o-tower.co.jp/okhsympo/top-index.html

Okhotsk Sea and Polar Oceans Research Vol. 3 2019

Okhotsk Sea and Polar Oceans Research

Published by the Okhotsk Sea and Polar Oceans Research Association (OSPORA)
Mombetsu City, Hokkaido, Japan